Effect of Sn substituting for Sb on the low-temperature transport properties of ytterbium-filled skutterudites

J. Yang,[1] D. T. Morelli,[2] G. P. Meisner,[1] W. Chen,[3] J. S. Dyck,[3] and C. Uher[3]
[1]*Materials and Processes Laboratory, GM R&D and Planning, Warren, Michigan 48090*
[2]*Delphi Corporation Research Labs, Shelby Township, Michigan 48315*
[3]*Department of Physics, University of Michigan, Ann Arbor, Michigan 48109*
(Received 20 June 2002; revised manuscript received 12 December 2002; published 24 April 2003)

We examine the effect of alloying Sn on the Sb site of ytterbium-filled skutterudites, a promising class of thermoelectric materials. We report measurements of the Hall effect, electrical resistivity, Seebeck coefficient, and thermal conductivity between 2 and 300 K on two series of samples having different ytterbium filling fractions: $Yb_{0.19}Co_4Sb_{12-x}Sn_x$, with $x=0$, 0.05, 0.1, and 0.2, and $Yb_{0.5}Co_4Sb_{12-x}Sn_x$, with $x=0.5$, 0.6, 0.8, 0.83, and 0.9. We find that the substitution of Sn does not lower the electron concentration of these samples, but rather gives rise to a *p*-type carrier. Hall measurement data for $Yb_{0.5}Co_4Sb_{11.17}Sn_{0.83}$ can be understood in the context of two-carrier electrical conduction. Although the thermal conductivity of these ytterbium-filled skutterudites is significantly suppressed from that of the unfilled $CoSb_3$, it is nearly independent of the Sn concentration. The role of phonon-point defect scattering and phonon resonance scattering in reducing the lattice thermal conductivity of the Yb-filled samples is assessed by a theoretical model.

DOI: 10.1103/PhysRevB.67.165207 PACS number(s): 63.20.−e, 66.70.+f, 72.20.−i

INTRODUCTION

Skutterudite compounds have been extensively studied over the past several years for their potential advanced thermoelectric applications by researchers worldwide.[1,2] The efficiency of a thermoelectric material is characterized by the dimensionless thermoelectric figure of merit, *ZT*, defined as

$$ZT=\frac{S^2T}{\rho\kappa_{\text{total}}}=\frac{S^2T}{\rho(\kappa_L+\kappa_e)},$$

where *S*, *T*, ρ, κ_{total}, κ_L, and κ_e are the Seebeck coefficient, absolute temperature, electrical resistivity, total thermal conductivity, lattice thermal conductivity, and electronic thermal conductivity, respectively. The energy conversion efficiency of a thermoelectric material increases with increasing *ZT*. A good thermoelectric material should possess a large Seebeck coefficient, a low electrical resistivity, and a low total thermal conductivity. Binary skutterudite compounds crystallize in a body-centered-cubic structure with space group $Im3$ and have the form MX_3, where *M* is Co, Rh, or Ir, and *X* is P, As, or Sb. Binary skutterudites are semiconductors with small band gaps of ~100 meV, high carrier mobilities, and modest Seebeck coefficients. Despite their excellent electronic properties, binary skutterudites have thermal conductivities that are too high to compete with state-of-the-art thermoelectric materials. Filled skutterudites can be formed by inserting guest atoms interstitially into the large voids in the crystal structure of the binary compounds. The lattice thermal conductivities of the filled skutterudites are significantly reduced over a wide temperature range compared to the binary skutterudites,[3–7] making them viable candidates for thermoelectric power generation.[8] The chemical composition for filled skutterudites can be written as $G_yM_4X_{12}$, where *G* represents a guest atom and *y* is its filling fraction. In the past several years, a number of filling elements have been explored in an effort to optimize the thermoelectric figure of merit of these compounds, including most of the rare earth elements[1,2] Ba,[9] Tl,[10] and Sn.[11] Recently, higher figures of merit were reported for Yb-filled skutterudites.[12,13] Specifically, the $Yb_{0.19}Co_4Sb_{12}$ composition reaches $ZT=1.0$ at 600 K.[12] Interestingly, even though *ZT* of $Yb_{0.066}Co_4Sb_{12}$ is lower than that of $Yb_{0.19}Co_4Sb_{12}$ over the entire temperature range,[12] the room temperature power factor (S^2/ρ) of $Yb_{0.066}Co_4Sb_{12}$ is 39.7 μW/cm K^2, about 20% higher than that of $Yb_{0.19}Co_4Sb_{12}$ (33.3 μW/cm K^2). Our Hall measurements indicate that the room temperature carrier concentration is 4.9×10^{19} cm^{-3} for $Yb_{0.066}Co_4Sb_{12}$ and 1.7×10^{20} cm^{-3} for $Yb_{0.19}Co_4Sb_{12}$.[12] It has been suggested that the power factor of *n*-type skutterudites is maximum at a carrier concentration between 1×10^{19} and 5×10^{19} cm^{-3}.[14] In our previous studies, we demonstrated that the lattice thermal conductivity of filled skutterudites is minimized with a filling fraction $y\sim0.5$,[15] and Fe alloying on the Co site of the skutterudites (which allows the skutterudite structure to accommodate a higher concentration of guest atoms) reduces significantly the carrier mobility.[16] In light of our previous studies and the recent encouraging results by others on Yb-filled skutterudites,[12–14] we carried out a study on a series of polycrystalline samples with two different Yb filling fractions: $Yb_{0.19}Co_4Sb_{12-x}Sn_x$ with $x=0$, 0.05, 0.1, and 0.2, and $Yb_{0.5}Co_4Sb_{12-x}Sn_x$ with $x=0.5$, 0.7, 0.8, 0.83, and 0.9. In addition to the dramatic reduction of the lattice thermal conductivity upon void filling with Yb atoms, the thermoelectric properties of these compounds are influenced by the presence of Sn substituting on the Sb site—the effect that is the focus of this paper.

EXPERIMENTAL TECHNIQUES

Polycrystalline samples of the form $Yb_yCo_4Sb_{12-x}Sn_x$ were synthesized by melting stoichiometric amounts of high purity constituents in sealed quartz tubes, which were filled with ultrahigh purity argon at 25 kPa pressure. The tubes

were then loaded into a box furnace, heated to 600 °C at 5 °C/min, soaked at 600 °C for 30 min, heated slowly (2 °C/min) to 950 °C, soaked at 950 °C for 48 h, annealed at 650 °C for 72 h, and finally cooled to room temperature at 2 °C/min. The middle sections of the final ingots were cut for transport and structural characterization. X-ray powder diffraction spectra were collected in order to determine the crystalline phases and the lattice parameters, using Cu $K\alpha$ radiation and scanning from 10° to 140° 2θ with a step time of 4 sec and a step interval of 0.04°. Sample compositions were analyzed by electron probe mircroanalysis (EPMA). Density measurements were performed with an ACCUPYC 1330 pycnometer. Thermal conductivity, Seebeck coefficient, and resistivity measurements were made from 1.7 to 300 K in a cryostat with a radiation shield. Hall effect measurements were made in a cryostat equipped with a 5.5 T magnet using a standard four-probe ac technique. Details of the experiment were described elsewhere.[17]

RESULTS AND DISCUSSION

We can definitely identify the predominant skutterudite phase for all samples in the x-ray powder diffraction experiment. Our x-ray powder diffraction data also reveal the presence of impurity phases of $CoSb_2$ and $YbSb_2$. The ratio between the highest impurity peak and the highest skutterudite peak is about a few percent; we therefore estimate all the samples contain a few percent of impurity phases. This is confirmed by our EPMA, which gives actual y and x values within 10% of their nominal values. The chemical formulas in the rest of the paper will refer to the nominal stoichiometry of the samples. Similar results for stoichiometry were reported by others.[18] All samples are at least 95% dense.

A. Hall effect measurements

All samples, except for $Yb_{0.5}Co_4Sb_{11.1}Sn_{0.9}$, exhibit n-type electrical conduction at room temperature with carrier concentrations of approximately 6.0×10^{19} and 5.0×10^{21} cm^{-3} for $Yb_{0.19}Co_4Sb_{12-x}Sn_x$ and $Yb_{0.5}Co_4Sb_{12-x}Sn_x$ ($x\leqslant0.8$), respectively. Figure 1 displays the temperature dependence of the carrier concentration for the $Yb_{0.5}Co_4Sb_{12-x}Sn_x$ samples. Their Hall (transverse) resistance R_{xy} is a linear function of the external magnetic field at all temperatures, indicating that the electrical transport is most likely dominated by a single carrier type. The Hall data for pure $CoSb_3$ from Ref. 19 is also plotted for comparison. The samples with $x\leqslant0.8$ shown in Fig. 1 have electron concentrations of the order of 10^{21} cm^{-3} over the entire temperature range, and all have weak temperature dependences. This suggests that they are all heavily n doped, which is expected for the Yb-filled skutterudites. Surprisingly, as the Sn content increases ($x\leqslant0.8$), the electron concentration does not decrease as one would expect upon substituting a group IV element for a group V element. This is also observed for the $Yb_{0.19}Co_4Sb_{12-x}Sn_x$ samples. Interestingly, as x increases from 0.8 to 0.9 for $Yb_{0.5}Co_4Sb_{12-x}Sn_x$, we notice a sharp transition in carrier concentration from heavily n doped ($x=0.8$) to heavily p doped ($x=0.9$).

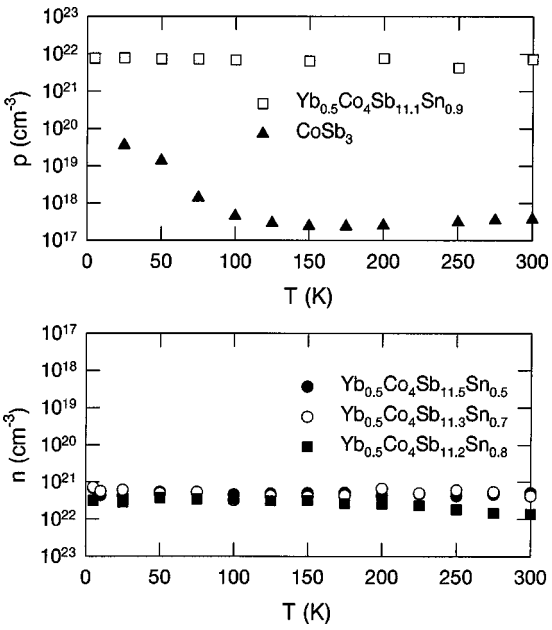

FIG. 1. Temperature dependence of the carrier concentration for $Yb_{0.5}Co_4Sb_{12-x}Sn_x$ samples, all of which are n-type, except for $Yb_{0.5}Co_4Sb_{11.1}Sn_{0.9}$. For comparison, data for $CoSb_3$ from Ref. 19 are also plotted.

The low temperature Hall data of $Yb_{0.5}Co_4Sb_{11.17}Sn_{0.83}$, plotted in Fig. 2, may shed some light on these puzzles. Figure 2 displays the Hall resistance R_{xy} as a function of the magnetic field H between 5 and 100 K for $Yb_{0.5}Co_4Sb_{11.17}Sn_{0.83}$. At each temperature, R_{xy} decreases with increasing H at low H. R_{xy} then reaches a minimum and finally attains a positive slope $\partial R_{xy}/\partial H$ at high magnetic field. This is indicative of a two-carrier electrical transport consisting of both n- and p-type carriers where the carrier mobility of the n-type carrier is higher than that of the p-type

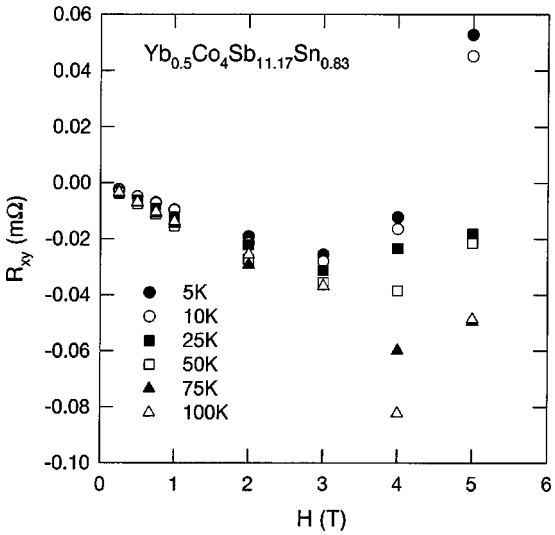

FIG. 2. Magnetic field dependence of the Hall resistance R_{xy} for $Yb_{0.5}Co_4Sb_{11.17}Sn_{0.83}$ between 5 and 100 K.

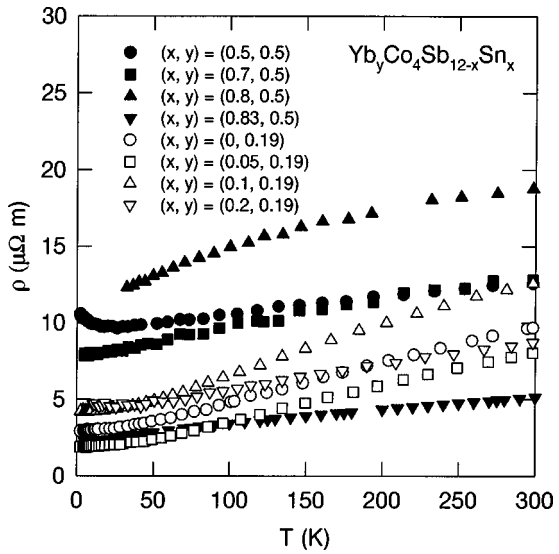

FIG. 3. Temperature dependence of the electrical resistivity for $Yb_yCo_4Sb_{12-x}Sn_x$.

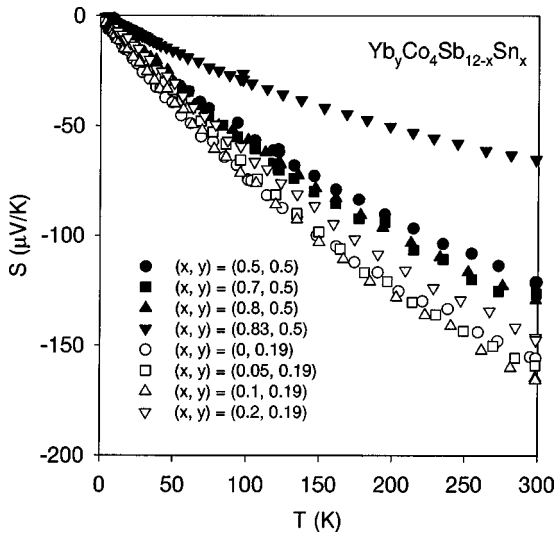

FIG. 4. Temperature dependence of the Seebeck coefficient for $Yb_yCo_4Sb_{12-x}Sn_x$.

carrier at any given temperature. As temperature increases, $\partial R_{xy}/\partial H > 0$ occurs at higher magnetic field H.

At even higher temperatures, R_{xy} becomes a linear function of H with $\partial R_{xy}/\partial H < 0$ over the whole range of H. This indicates that the mobility of the *p*-type carrier decreases rapidly as temperature increases. At $T > 200$ K, a 5 T magnetic field is not sufficient to detect the *p*-type carriers. From our Hall data, we believe that alloying Sn on the Sb site of skutterudites does not lower the Fermi level with respect to the conduction band, which would result in lowering the carrier concentration; rather it gives rise to a *p* band. We speculate that further increasing the Sn content increases the mobility of the *p* band, leading to electrical conduction dominated by *p*-type carriers. This point of view is further corroborated by *p*-type carrier dominated electrical conduction in our $Yb_{0.5}Co_4Sb_{11.1}Sn_{0.9}$ sample plotted in Fig. 1, and in the $Yb_{0.5}Co_4Sb_{11}Sn_1$ and $Yb_{0.5}Co_4Sb_{10}Sn_2$ samples from Ref. 18. The exact location of the *p* band is not known at this time, and band structure calculations would be very helpful in clarifying its existence and location.

B. Resistivity and Seebeck coefficient

Temperature dependence of the electrical resistivity for all the $Yb_yCo_4Sb_{12-x}Sn_x$ samples is shown in Fig. 3. Except for the $Yb_{0.5}Co_4Sb_{11.5}Sn_{0.5}$ sample (filled circles), which has a semiconducting behavior at low temperature, the electrical resistivity for all the samples has a metallic behavior over the entire temperature range. This is typical for heavily doped semiconductors. The resistivities for $Yb_{0.19}Co_4Sb_{12-x}Sn_x$ are lower than that of $Yb_{0.5}Co_4Sb_{12-x}Sn_x$, except that $Yb_{0.5}Co_4Sb_{11.17}Sn_{0.83}$ has the lowest resistivity among all samples. The lower resistivity for $Yb_{0.19}Co_4Sb_{12-x}Sn_x$ is due to their much higher electron mobility compared to that of $Yb_{0.5}Co_4Sb_{12-x}Sn_x$. For $Yb_{0.5}Co_4Sb_{11.17}Sn_{0.83}$, the addition of the *p*-type carriers results in an increase in the electrical conduction, and therefore a significant lowering of the electrical resistivity. The room temperature resistivity values are close to those reported in Ref. 18.

Figure 4 depicts the temperature dependence of the Seebeck coefficient for the $Yb_yCo_4Sb_{12-x}Sn_x$ samples. We find $S < 0$ for all the samples in the entire temperature range, indicating the carriers are dominantly *n*-type in agreement with the Hall data. In the case of the $y = 0.19$ series, both the magnitude and temperature dependences of the Seebeck coefficient are nearly independent of the Sn concentration, with room temperature values clustered between -140 and -160 μV/K. A similar behavior is seen in the $y = 0.5$ series for samples with $x \leqslant 0.8$, with all samples having a room temperature Seebeck coefficient between -120 and -130 μV/K. This is, again, consistent with our Hall results described earlier, because the Seebeck coefficient is, to a first approximation, determined by the position of the Fermi level with respect to the band structure. Our Hall data suggest that alloying Sn on the Sb site does not alter the relative position of the Fermi level with respect to the conduction band. Therefore, we do not expect significant changes in the Seebeck coefficient for $x \leqslant 0.8$, and this is borne out by the results shown in Fig. 4. The $x = 0.83$ sample has a much smaller room temperature Seebeck coefficient value, -65.3 μV/K, and reflects the trend in the Hall data for the sample. In the presence of the *p*-type carriers in addition to the *n*-type carriers from the conduction band in this sample, the total Seebeck coefficient can be expressed as

$$S = \frac{\sigma_n S_n + \sigma_p S_p}{\sigma_n + \sigma_p}, \tag{1}$$

where $S_{n,p}$ and $\sigma_{n,p}$ are the Seebeck coefficients and the electrical conductivities for the *n*- and *p*-type carriers, respectively. Because of the opposite signs of S_n and S_p, $|S|$ will be smaller than $|S_n|$.

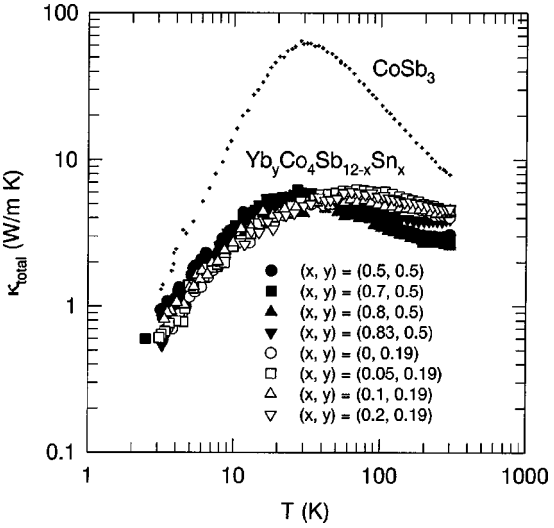

FIG. 5. Temperature dependence of the total thermal conductivity for $Yb_yCo_4Sb_{12-x}Sn_x$. For comparison, data for $CoSb_3$ (from Ref. 20) are also plotted.

C. Thermal conductivity

Thermal conductivity is another crucial factor that determines the thermoelectric properties of these compounds. Our thermal conductivity data are plotted in Fig. 5 along with the data for $CoSb_3$ for comparison.[20] The thermal conductivity of the Yb-filled skutterudites is significantly lower than their binary parent compound $CoSb_3$ over the entire temperature range. It is useful to isolate the lattice thermal conductivity κ_L by subtracting the electronic component as determined by the Wiedemann-Franz Law; the results are shown in Fig. 6. Within each family of compounds, the addition of Sn leaves the lattice thermal conductivity practically unaltered. This is because the Sn substitutes for Sb and the resulting mass difference (less than 3%) causes very little additional phonon scattering. Consistent with the large body of literature already developed on filled skutterudites, Yb filling causes a reduction in lattice thermal conductivity; at room temperature κ_L is on the order of 3.5–4.0 W/m K for $y=0.19$ and 2.2–2.6 W/m K for $y=0.5$. Increasing Yb filling also alters the temperature at which κ_L peaks (T_{max}). $T_{max}=29$, 68, and 27 K for $y=0$, 0.19, and 0.5, respectively. This is different from what we observed in the κ_L of Fe- and Ni-doped $CoSb_3$,[16,20] where the increasing amount of impurities increases scattering of lattice phonons by point defects[16] and electrons,[20] respectively, resulting in the reduction of κ_L. In both cases, T_{max} increases as the impurity level increases.

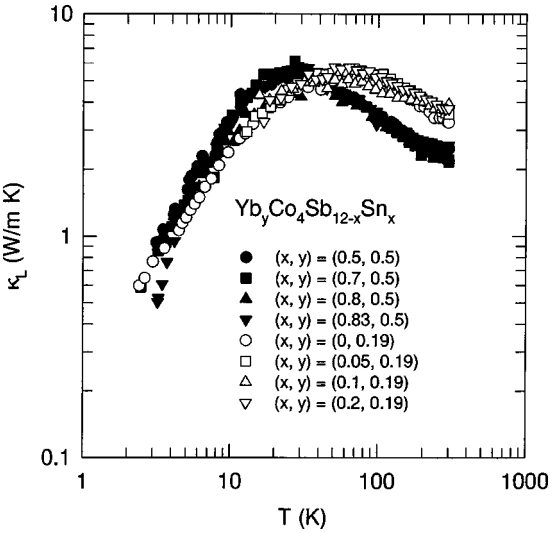

FIG. 6. Temperature dependence of the lattice thermal conductivity for $Yb_yCo_4Sb_{12-x}Sn_x$.

We modeled our κ_L data using the Debye approximation[21,22]

$$\kappa_L=\frac{k_B}{2\pi^2 v}\left(\frac{k_B}{\hbar}\right)^3 T^3\int_0^{\theta_D/T}\frac{x^4e^x}{\tau_c^{-1}(e^x-1)}dx, \qquad (2)$$

where $x=\hbar\omega/k_BT$ is dimensionless, ω is the phonon frequency, k_B is the Boltzmann constant, $\hbar$ is the reduced Planck constant, θ_D is the Debye temperature, v is the velocity of sound, and τ_c is the phonon scattering relaxation time. The overall phonon relaxation rate can be written as

$$\tau_c^{-1}=\frac{v}{L}+A\omega^4+B\omega^2Te^{-\theta_D/3T}+\frac{C\omega^2}{(\omega_0^2-\omega^2)^2}, \qquad (3)$$

where L is the grain size, and A, B, and C are the fitting parameters. The terms on the right side of the Eq. (3) represent grain-boundary, point defect, phonon-phonon Umklapp, and phonon resonance scatterings, respectively. The interaction between the lattice phonons and the Yb fillers is modeled by an additional phonon resonance scattering term. The phonon resonance term was employed previously to describe phonon scattering in KNO_2 containing KCl crystals,[23] and in clathrates.[24] C is supposed to be proportional to the concentration of the Yb fillers,[23] and ω_0 is the resonance frequency. As we have shown in Fig. 6, κ_L is drastically changed upon Yb filling, but independent of the Sn content x. One only needs to fit κ_L data for different y values. All samples plotted in Fig. 6 were fit using Eqs. (2) and (3), however, to assess the accuracy of the fitting parameters. The fitting parameters are listed in Table I. Figure 7 shows the experimental κ_L data with the theoretical fit for $CoSb_3$ from Ref. 20, $Yb_{0.19}Co_4Sb_{12}$, and $Yb_{0.5}Co_4Sb_{11.5}Sn_{0.5}$. The solid lines fit the experimental data very well for all three samples over the entire two orders of magnitude temperature span. The deviation between the experimental data and the calculation for $Yb_{0.5}Co_4Sb_{11.5}Sn_{0.5}$ near room temperature is attributed to the possible radiation losses, similar to those observed previously.[16,20] The grain size determined from the fits to the data (Table I) agree with the backscattered electron image results. A, B, C, and ω_0 values listed in Table I vary within approximately 20% for the same Yb filling fraction y. This indicates that the error bars of these fitting parameters are about 20% of their listed values in Table I. Prefactor A for point defect scattering emerging from the fits to the data is plotted in Fig. 8(a) as a function of $y(1-y)$. A varies linearly with $y(1-y)$ which indicates that the phonon-point defect scattering is mainly due to the mass-fluctuation on the Yb sites between Yb_y and $\square_{1-y}$ ($\square$ represents a lattice vacancy), a picture proposed by Ref. 15. We were not able to fit

TABLE I. Lattice thermal conductivity fitting parameters for $CoSb_3$ (Ref. 20), $Yb_{0.19}Co_4Sb_{12-x}Sn_x$, and $Yb_{0.5}Co_4Sb_{12-x}Sn_x$ as defined by Eqs. (2) and (3).

Sample	L (μm)	A (10^{-43} s^3)	B (10^{-18} s K^{-1})	C (10^{33} s^{-3})	ω_0 (THz)
$CoSb_3$	5.772	2.591	5.375	0	—
$Yb_{0.19}Co_4Sb_{12}$	29.03	150.1	2.593	3.102	2.384
$Yb_{0.19}Co_4Sb_{11.95}Sn_{0.05}$	27.6	127.8	2.454	3.592	2.309
$Yb_{0.19}Co_4Sb_{11.9}Sn_{0.1}$	6.821	150.1	2.721	3.428	3.601
$Yb_{0.19}Co_4Sb_{11.8}Sn_{0.2}$	9.757	133.5	2.089	2.132	1.568
$Yb_{0.5}Co_4Sb_{11.5}Sn_{0.5}$	8.820	202.4	7.030	7.317	6.060
$Yb_{0.5}Co_4Sb_{11.3}Sn_{0.7}$	7.439	187.6	8.057	7.361	7.308
$Yb_{0.5}Co_4Sb_{11.2}Sn_{0.8}$	7.699	231.5	5.391	7.467	5.314
$Yb_{0.5}Co_4Sb_{11.17}Sn_{0.83}$	8.581	200.8	6.976	7.241	8.809

the data for all three samples in Fig. 7 using a single B value, and there is no obvious trend for B as a function of the Yb filling fraction y. B is a function of the mean atomic weight, the lattice parameter, θ_D the average number of atoms in the unit cell, and the Grüneisen constant γ.[25,26] γ is a measure of the lattice anharmonicity. Because we do not know the values of θ_D and γ for these series of samples, the exact y dependence of B is not clear. The values of B listed in Table I are about the same order of magnitude. In addition, B and ω_0 for the $y=0.5$ samples are about 2–3 times larger than those of the $y=0.19$ samples. This is attributed to the lattice parameter increase due to the increase of both y and x. Furthermore, our magnetic susceptibility, Mössbauer spectroscopy, and X-ray absorption near-edge structure spectroscopy (XANES) data on the same samples suggest an evolution of Yb valence parallels an increase in the lattice parameter and hence in the ratio of the Yb ion size versus the void size as the Sn content increases.[27] It is reasonable to believe ω_0 does change as a function of both y and x. Both the phonon-phonon Umklapp scattering and the phonon resonance scattering are very sensitive to the size of the unit cell. In Fig. 8(b), the prefactor C for phonon resonance scattering is plotted as a function of the Yb filling fraction y, and increases linearly with increasing y. The partial relaxation rate for phonon resonance scattering in Eq. (3) was derived for a simple mechanical oscillator. Therefore C should be proportional to the concentration of the oscillators. Figures 7 and 8(b) suggest that, apart from the point defect scattering, the additional phonon scattering due to Yb filling can be well described by the phonon resonance scattering term in Eq. (3), and the phonon resonance scattering increases linearly with increasing Yb concentration y at least for $y \leqslant 0.5$.

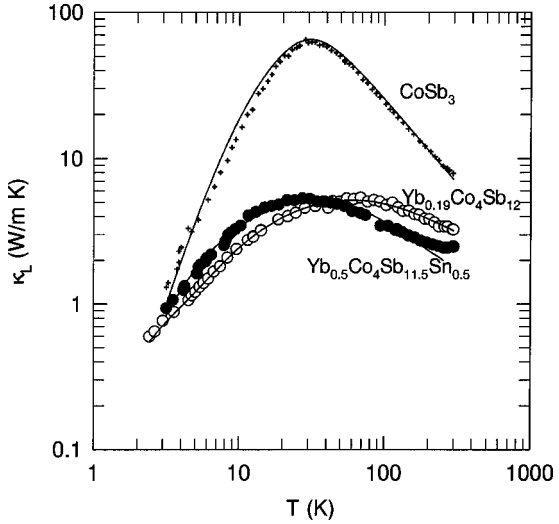

FIG. 7. Temperature dependence of the lattice thermal conductivity for $CoSb_3$ (Ref. 20), $Yb_{0.19}Co_4Sb_{12}$, and $Yb_{0.5}Co_4Sb_{11.5}Sn_{0.5}$. The symbols are the experimental data, and the solid lines represent the calculation based on Eqs. (2) and (3).

SUMMARY

We have studied the effect of Sn alloying on the Sb site of Yb-filled skutterudites $Yb_yCo_4Sb_{12-x}Sn_x$ by measuring the

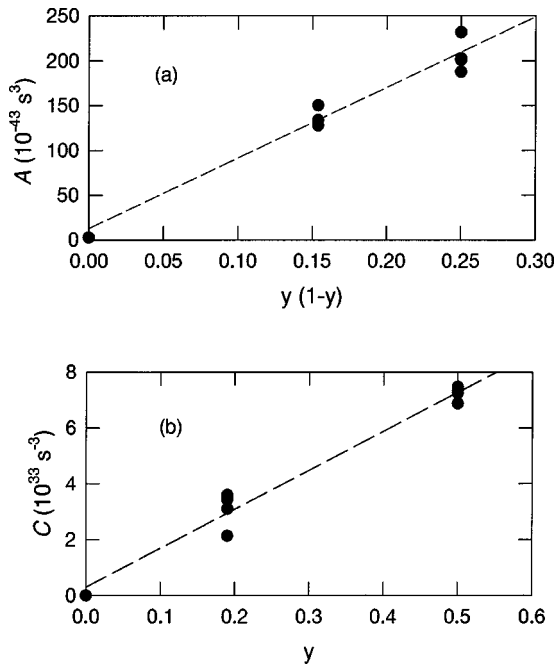

FIG. 8. (a) Prefactor A for point defect scattering as a function of $y(1-y)$, and (b) prefactor C for phonon resonance scattering as a function of y. Dashed lines are results of linear fits in both (a) and (b).

Hall effect, electrical resistivity, Seebeck coefficient, and thermal conductivity on series of samples with $y = 0.19$ and 0.50. Our data suggest that alloying Sn on the Sb site does not lower the Fermi level with respect to the conduction band, but instead gives rise to a *p*-type band for a sufficiently large Sn content *x*. The Hall data, electrical resistivity and Seebeck coefficient of $Yb_{0.5}Co_4Sb_{11.17}Sn_{0.83}$ can be understood in the framework of two-carrier electrical conduction. The lattice thermal conductivity of the Yb-filled skutterudites is significantly lower than the parent binary compound $CoSb_3$ but is nearly independent of Sn concentration. Our theoretical analysis indicates that (a) the increasing Yb filling increases both phonon point defect scattering and phonon resonance scattering, (b) point defect scattering is mainly due to the mass fluctuation on the Yb sites between Yb atoms and the vacancies, and (c) phonon resonance scattering increases linearly with increasing Yb content in the *y* range we studied. Since alloying Sn on the Sb site is unable to alter the Fermi level, it is not an effective method for optimizing the thermoelectric power factor of the Yb-filled skutterudites.

ACKNOWLEDGMENTS

J.Y. and G.P.M. want to thank Dr. J. F. Herbst and Dr. K. C. Taylor for their support and encouragement throughout this work. The authors would like to thank M. P. Balogh and R. A. Waldo for assistance in x-ray diffraction and EPMA measurements. The work was also supported in part by DARPA under Contract No. 00014-98-3-0011.

[1] C. Uher, in *Recent Trends in Thermoelectric Materials Research I*, Semiconductors and Semimetals, Vol. 69, edited by T. M. Tritt (Academic, San Diego, 2000), p. 139.
[2] G. S. Nolas, D. T. Morelli, and T. M. Tritt, Annu. Rev. Mater. Sci. **29**, 89 (1999).
[3] D. T. Morelli and G. P. Meisner, J. Appl. Phys. **77**, 3777 (1995).
[4] G. S. Nolas, G. A. Slack, D. T. Morelli, T. M. Tritt, and A. C. Ehrlich, J. Appl. Phys. **79**, 4002 (1996).
[5] B. C. Sales, D. Mandrus, and R. K. Williams, Science **272**, 1325 (1996).
[6] B. Chen, J. Xu, C. Uher, D. T. Morelli, G. P. Meisner, J.-P. Fleurial, T. Caillat, and A. Borshchevsky, Phys. Rev. B **55**, 1476 (1997).
[7] D. T. Morelli, G. P. Meisner, B. Chen, S. Hu, and C. Uher, Phys. Rev. B **56**, 7376 (1997).
[8] J.-P. Fleurial, A. Borshchevsky, T. Caillat, D. T. Morelli, and G. P. Meisner, U.S. Patent No. 6,069,12 (2000).
[9] X. Tang, L. Chen, G. Takashi, and H. Toshio, J. Jpn. Soc. Powder Powder Metall. **47**, 1165 (2000).
[10] B. C. Sales, B. C. Chakoumakos, and D. Mandrus, Phys. Rev. B **61**, 2475 (2000).
[11] G. S. Nolas, H. Takizawa, T. Endo, H. Sellinschegg, and D. C. Johnson, Appl. Phys. Lett. **77**, 52 (2000).
[12] G. S. Nolas, M. Kaeser, R. T. Littleton IV, and T. M. Tritt, Appl. Phys. Lett. **77**, 1855 (2000).
[13] B. C. Sales, B. C. Chakoumakos, and D. Mandrus, in *Thermoelectric Materials 2000–The Next Generation Materials for Small-Scale Refrigeration and Power Generation Applications*, edited by T. M. Tritt, G. S. Nolas, G. D. Mahan, D. Mandrus, and M. G. Kanatzidis, MRS Symposia Proceedings No. 626 (Materials Research Society, Pittsburgh, 2000), p. Z7.1.1.
[14] G. S. Nolas, M. Kaeser, R. T. Littleton IV, and T. M. Tritt, H. Sellinschegg, D. C. Johnson, and E. Nelson, in *Thermoelectric Materials 2000–The Next Generation Materials for Small-Scale Refrigeration and Power Generation Applications* (Ref. 13), p. Z10.1.1.
[15] G. P. Meisner, D. T. Morelli, S. Hu, J. Yang, and C. Uher, Phys. Rev. Lett. **80**, 3551 (1998).
[16] J. Yang, G. P. Meisner, D. T. Morelli, and C. Uher, Phys. Rev. B **63**, 014410 (2001).
[17] J. Yang, Ph.D. thesis (University of Michigan, Ann Arbor, MI, 2000).
[18] N. R. Dilley, E. D. Bauer, M. B. Maple, and B. C. Sales, J. Appl. Phys. **88**, 1948 (2000).
[19] J. S. Dyck, W. Chen, J. Yang, G. P. Meisner, and C. Uher, Phys. Rev. B **65**, 115204 (2002).
[20] J. Yang, D. T. Morelli, G. P. Meisner, W. Chen, J. S. Dyck, and C. Uher, Phys. Rev. B **65**, 094115 (2002).
[21] J. Callaway, Phys. Rev. **113**, 1046 (1959).
[22] J. Callaway, Phys. Rev. **120**, 1149 (1960).
[23] R. O. Pohl, Phys. Rev. Lett. **8**, 481 (1962).
[24] J. L. Cohn, G. S. Nolas, V. Fessatidis, T. H. Metcalf, and G. A. Slack, Phys. Rev. Lett. **82**, 779 (1999).
[25] G. A. Slack, and V. G. Tsoukala, J. Appl. Phys. **76**, 1665 (1994).
[26] J. M. Ziman, *Electrons and Phonons* (Clarendon, Oxford, 1960).
[27] F. Grandjean, G. J. Long, B. Mahieu, J. Yang, G. P. Meisner, and D. T. Morelli (unpublished).